Computers Fluids Vol. 23, No. 1, pp. 103–114, 1994
Printed in Great Britain.

0045-7930/94 $6.00 + 0.00

EFFICIENT NUMERICAL METHOD FOR SIMULATION OF SUPERSONIC VISCOUS FLOW PAST A BLUNTED BODY AT A SMALL ANGLE OF ATTACK

G. A. TIRSKII, S. V. UTYUZHNIKOV† and N. K. YAMALEEV
Department of Computational Mathematics, Moscow Institute of Physics & Technology, Dolgoprudny, Moscow 141700, Russia

(Received 6 February 1992; in revised form 2 October 1992)

Abstract—For solving the three-dimensional (3-D) full viscous shock-layer (FVSL) equations in a body-oriented coordinate system, an asymptotic method is used with the angle of attack as a small parameter. In using a small parameter method, the (3-D) FVSL system is separated into an axisymmetric set and a linear 2-D set of equations. The method of global iterations was used to solve both the axisymmetric and linearized sets of equations. Global iterations were carried out on the pressure gradient tangential component and on the shock wave angle. The method is used uniformly for both the blunted and conic parts of the body. The shock wave angle was found by using the Rankine–Hugoniot boundary condition for the normal component of the velocity. A computational grid adapted to the solution was used in solving both systems of equations. The comparison of this approach with 3-D implicit time-marching methods shows that the time necessary for the calculation in the 3-D case is about 100 times less, while the accuracy of the calculations is essentially the same. Also, the small parameter method enables one to find a one-parameter family of solutions; the parameter in question is the angle of attack.

NOMENCLATURE

u = Tangential velocity component, u'/V_∞
v = Normal velocity component, v/V_∞
w = Transverse velocity component, w'/V_∞
V_∞ = Free-stream velocity
h = Nondimensional specific enthalpy, h'/H_∞
H = Nondimensional total enthalpy, H'/H_∞
H_∞ = Free-stream total enthalpy
T = Nondimensional temperature, T'/T_∞
T_∞ = Free-stream temperature
P = Nondimensional pressure, $P'/\rho_\infty V_\infty^2$
ρ = Nondimensional density, ρ'/ρ_∞
ρ_∞ = Free-stream density
μ = Nondimensional viscosity, μ'/μ_∞
μ_∞ = Free-stream viscosity
R_n = Nose radius
Re_∞ = Free-stream Reynolds number, $\rho_\infty V_\infty R_n/\mu_\infty$
M_∞ = Free-stream Mach number
γ = Ratio of specific heats
σ = Prandtl number
y_s = Shock standoff distance, y_s'/R_n
y = Normal coordinate, y'/R_n
x = Surface coordinate, x'/R_n
φ = Transverse coordinate
z = Axial coordinate, z'/R_n
n = Transformed coordinate given by equation (6)
ξ = Transformed coordinate given by equation (6)
ν = Transformed coordinate given by equation (6)
$r\mathrm{w}$ = Radius measured from the axis of symmetry to a point on the body surface, r_w'/R_n
æ = Local curvature, $æ'/R_n$
α = Body surface angle measured from the body axis
ϵ = Angle of attack
C_H = Heat-transfer coefficient, $(2\mu_w/\sigma\mathrm{Re}_\infty)(\partial h/\partial y)$
C_x = Drag coefficient
C_y = Lift coefficient
M_z = Pitching moment coefficient

Superscripts

$'$ = Dimensional quantities
(k) = Coefficient number of the Fourier series expansion

Subscripts

0 = Axisymmetric quantities
w = Conditions at the body surface
s = Conditions at the shock surface
g = Quantities calculated on the previous global iteration
c = Quantities calculated on the current global iteration

INTRODUCTION

The purpose of this paper is to study the viscous flow over spherically blunted bodies at small angles of attack. The full viscous shock-layer equations (FVSL) are used to describe the flow field. In these equations, terms up to the second order in the inverse square root of the Reynolds number are retained from both the viscous and inviscid points of view. The shock wave is treated as a discontinuity, across which the Rankine–Hugoniot relations are used to compute the flow conditions behind the shock.

†To whom all correspondence should be addressed.

For solving three-dimensional (3-D) FVSL equations in the body-oriented coordinate system an asymptotic method is used, with the angle of attack as a small parameter. The basic idea of the method is to represent a 3-D solution as the sum of an axisymmetric solution and a linear disturbance, the latter being represented as a Fourier series expansion. In using a small parameter method, the 3-D FVSL equations are separated into an axisymmetric set of equations and a linear 2-D set of equations. The practical importance of this simplification is obvious. The application of a numerical method for the solution of 3-D FVSL equations needs a lot of computer time and may also lead to a loss of accuracy in the numerical results in the case of small angles of attack. A simple analysis shows that a small disturbance in the surface pressure distribution may lead to significant errors in the aerodynamic lift force.

A new numerical method based on global iterations was developed for the solution of both the axisymmetric and linearized sets of equations. Global iterations were carried out with respect to the pressure gradient tangential component and the shock wave angle. The method is used in the same way for both the blunted and conic parts of the body. The shock wave angle was found using the Rankine–Hugoniot boundary condition for the normal component of the velocity.

For the solution of the axisymmetric set of equations a finite-difference method of second order in the tangential coordinate and of fourth order in the normal coordinate is applied. For the linearized set of equations a finite-difference method of the first order in the tangential coordinate and of fourth order in the normal coordinate is used. A computational grid adapted to the solution is used in solving both sets of equations.

The comparison of this approach with 3-D implicit time-marching methods shows that the time necessary for the calculation in the 3-D case is about 100 times less; the accuracy of the calculations is the same. Also, the small parameter method enables one to find a one-parameter family of solutions; the parameter in question is the angle of attack.

The numerical results obtained for quantities such as the shock standoff distance, surface pressure distribution and heating rates compare well with the available experimental results. The calculation time does not change appreciably over a wide range of Mach numbers ($M_\infty > 3$) and Reynolds numbers ($10^2 \leqslant Re_\infty \leqslant 10^7$).

GOVERNING EQUATIONS

The basic equations used in the present analysis can be obtained from the steady full Navier–Stokes equations by retaining terms up to the second order in the inverse square root of the Reynolds number in both the viscous and inviscid regions [1]. For a steady flow without body forces and external heat sources, these equations can be written in a body-oriented coordinate system as:

$$\frac{\partial}{\partial x}(H_2\rho u)+\frac{\partial}{\partial \varphi}(H_1\rho w)+\frac{\partial}{\partial y}(H_1H_2\rho v)=0,$$

$$\rho\left[Du-\frac{w^2}{H_1H_2}\frac{\partial H_2}{\partial x}+\frac{uw}{H_1H_2}\frac{\partial H_1}{\partial \varphi}+\frac{uv}{H_1}\frac{\partial H_1}{\partial y}\right]=-\frac{1}{H_1}\frac{\partial P}{\partial x}+\frac{1}{H_1^2H_2\mathrm{Re}_\infty}\frac{\partial}{\partial y}\left[H_1^3H_2\mu\cdot\frac{\partial}{\partial y}\left(\frac{u}{H_1}\right)\right],$$

$$\rho\left[Dw+\frac{wu}{H_1H_2}\frac{\partial H_2}{\partial x}-\frac{u^2}{H_1H_2}\frac{\partial H_1}{\partial \varphi}+\frac{wv}{H_2}\frac{\partial H_2}{\partial y}\right]=-\frac{1}{H_2}\frac{\partial P}{\partial \varphi}+\frac{1}{H_1H_2^2\mathrm{Re}_\infty}\frac{\partial}{\partial y}\left[H_1H_2^3\mu\cdot\frac{\partial}{\partial y}\left(\frac{w}{H_2}\right)\right],$$

$$\rho\left[Dv-\frac{1}{H_1}\frac{\partial H_1}{\partial y}u^2-\frac{1}{H_2}\frac{\partial H_2}{\partial y}w^2\right]=-\frac{\partial P}{\partial y},$$

$$\rho DH=\frac{1}{H_1H_2}\frac{\partial}{\partial y}\left\{\frac{H_1H_2\mu}{\sigma\,\mathrm{Re}_\infty}\left[\frac{\partial H}{\partial y}+\frac{V_\infty^2(\sigma-1)}{2H_\infty}\cdot\frac{\partial(u^2+w^2)}{\partial y}-\frac{\sigma u^2V_\infty^2}{H_\infty H_1}\cdot\frac{\partial H_1}{\partial y}-\frac{\sigma w^2V_\infty^2}{H_\infty H_2}\cdot\frac{\partial H_2}{\partial y}\right]\right\}; \quad (1)$$

where

$$D=\frac{u}{H_1}\cdot\frac{\partial}{\partial x}+\frac{w}{H_2}\cdot\frac{\partial}{\partial \varphi}+v\cdot\frac{\partial}{\partial y}; \quad H=h+\frac{V_\infty^2}{2H_\infty}(u^2+w^2+v^2).$$

For the body-oriented coordinate system, the metric coefficients are given by

$$H_1 = 1 + y \cdot \text{æ}(x); \quad H_2 = r_w(x) + y \cdot \cos\alpha(x).$$

In addition to the abovementioned FVSL equations, an equation of state and viscosity law must be specified. For a perfect gas, the equation of state can be written as

$$h = \frac{\gamma P V_\infty^2}{(\gamma - 1)\rho H_\infty} \tag{2}$$

and in the present analysis either Sutherland's equation or the power law is used for the viscosity:

$$u \sim \frac{T^{3/2}}{T + 110.4},$$
$$\mu \sim T^p, \quad \text{where } 0.5 \leqslant p \leqslant 1. \tag{3}$$

BOUNDARY CONDITIONS

On the body surface the following conditions are imposed:

$$u(x, 0, \varphi) = v(x, 0, \varphi) = w(x, 0, \varphi) = 0; \quad H(x, 0, \varphi) = H_w^0. \tag{4}$$

The Rankine–Hugoniot relations are used at the outer boundary to determine the flow properties immediately behind the shock [2]. These relations in the body-oriented coordinate system are given as:

$$v_s = u_s \tan\beta_s + w_s \tan\gamma_s + K_s V_\infty(3),$$

$$P_s = \frac{1}{\gamma M_\infty^2} + \frac{V_\infty^2(3)(1 - K_s)}{1 + \tan^2\beta_s + \tan\gamma_s^2},$$

$$u_s = V_\infty(1)\cos^2\beta_s - \frac{w_s}{2}\sin 2\beta_s \cdot \tan\gamma_s - \frac{K_s}{2} V_\infty(3)\sin 2\beta_s + \frac{\mu_s}{\mathrm{Re}_\infty V_\infty(3)}\left[\frac{\partial u}{\partial y} - \frac{u}{H_1}\frac{\partial H_1}{\partial y}\right]_s,$$

$$w_s = V_\infty(2)\cos^2\gamma_s - \frac{u_s}{2}\sin 2\gamma_s \cdot \tan\beta_s - \frac{K_s}{2} V_\infty(3)\sin 2\gamma_s + \frac{\mu_s}{\mathrm{Re}_\infty V_\infty(3)}\left[\frac{\partial w}{\partial y} - \frac{w}{H_2}\frac{\partial H_2}{\partial y}\right]_s,$$

$$H_s = 1 + \frac{\mu_s}{\sigma\,\mathrm{Re}_\infty V_\infty(3)}\left[\frac{\partial H}{\partial y} + \frac{V_\infty^2(\sigma - 1)}{2H_\infty}\frac{\partial(u^2 + w^2)}{\partial y} - \frac{\sigma u^2 V_\infty^2}{H_\infty H_1}\frac{\partial H_1}{\partial y} - \frac{\sigma w^2 V_\infty^2}{H_\infty H_2}\frac{\partial H_2}{\partial y}\right],$$

$$V_\infty(1) = \cos\alpha \cdot \cos\epsilon + \sin\alpha \cdot \cos\varphi \cdot \sin\epsilon + \tan\beta_s \sin\alpha \cdot \cos\epsilon + \sin\epsilon \cdot \cos\varphi \cdot \cos\alpha,$$

$$V_\infty(2) = -\sin\varphi \cdot \sin\epsilon + \tan\gamma_s \cdot (-\sin\alpha \cdot \cos\epsilon + \sin\epsilon \cdot \cos\alpha \cdot \cos\varphi),$$

$$V_\infty(3) = -\frac{\cos\epsilon \cdot \sin\beta}{\cos\beta_s} + \frac{\sin\epsilon \cdot \cos\varphi \cdot \cos\beta}{\cos\beta_s} + \tan\gamma_s \cdot \sin\epsilon \cdot \sin\varphi.$$

$$\tan\beta_s = \frac{1}{H_{1s}}\frac{\partial y_s}{\partial x}, \quad \tan\gamma_s = \frac{1}{H_{2s}}\frac{\partial y_s}{\partial\varphi}, \quad K_s = \frac{1}{\rho_s}, \quad \beta = \beta_s + \alpha. \tag{5}$$

Where $V_\infty(i)$, $i = 1, 2, 3$, are the components of the free-stream velocity vector in the body-oriented coordinate system.

THE SMALL PARAMETER METHOD

The 3-D FVSL equations are solved by using a small parameter method. In order to use this method, the independent variable transformation is applied to the governing equations and the boundary conditions. This transformation maps the computational domain into a rectangular region in which both the shock and the body become the boundary mesh lines. The purpose of this transformation is to reduce the computational domain in the 3-D and axisymmetric cases to an identical form. This transformation is given by

$$\xi = x; \quad n = y/y_s; \quad v = \varphi; \quad y_s = y_s(x, \varphi). \tag{6}$$

For solving the 3-D FVSL equations the asymptotic small parameter method is used; the small parameter is the angle of attack [3, 4]. The main idea of this method is to represent a 3-D solution as the sum of an axisymmetric solution and a linear disturbance, the latter being represented as a Fourier series expansion. Hence the 3-D solution can be written as [cf. 4]:

$$\begin{aligned} F(\xi, n, v) &= F_0(\xi, n) + \epsilon F^{(1)}(\xi, n) \cdot \cos v + \epsilon^2 \cdot [F_0^{(2)}(\xi, n) + F_2^{(2)}(\xi, n) \cdot \cos 2v] + O(\epsilon^2), \\ w(\xi, n, v) &= \epsilon \cdot w^{(1)}(\xi, v) \cdot \sin v + \epsilon^2 \cdot w^{(2)}(\xi, \eta) \cdot \sin 2v + O(\epsilon^2), \\ F &= \{y_s, u, v, \rho, H, P\}, \end{aligned} \tag{7}$$

where F_0 is the axisymmetric solution and $F^{(1)}$, $F_0^{(2)}$, $F_2^{(2)}$, $w^{(1)}$ and $w^{(2)}$ are the coefficients of the Fourier series expansion.

In the present analysis only the first terms $F^{(1)}$ and $w^{(1)}$ of the Fourier series expansion are retained, since the higher order terms of this set are $O(\epsilon^2)$ [4].

Substituting equations (7) in equations (1)–(5) and separating the terms $O(1)$ and $O(\epsilon)$, the 3-D FVSL equations are split into an axisymmetric set and a linear 2-D set of equations, which are used to determine the first terms of the Fourier series expansion (this set of equations is given in the Appendix).

The practical importance of this simplification is obvious. The numerical solution of the 3-D FVSL equations is very expensive in terms of computer time and may lead to a loss of accuracy in the case of a small angle of attack. A simple analysis shows that a small disturbance in the surface pressure distribution may result in significant errors in the aerodynamic lift coefficient. The lift coefficient in the body-oriented coordinate system may be written as

$$C_y \sim \int_0^{2\pi} \int_0^{x_f} P_w(x, y, \varphi) \cdot \cos \alpha(x) \cdot \cos \varphi \cdot r_w(x) \, dx \, d\varphi, \tag{8}$$

where the viscous effects have been neglected. Substituting equations (7) in expression (8), C_y can be represented as

$$C_y \sim \epsilon \cdot \int_0^{x_f} P_w^{(1)}(x, y) \cdot \cos \alpha \cdot r_w(x) \, dx.$$

From this it follows that the absolute error in determining the lift coefficient C_y is of the order of the relative error in the Fourier coefficient $P_w^{(1)}$ (rather than of the order of the relative error in P_w). We have

$$\frac{\delta P_w^{(1)}}{P_w^{(1)}} \sim \frac{1}{\epsilon} \frac{\delta P_w}{P_w}. \tag{9}$$

Equation (9) explains the fact that, in using a 3-D code to determine the flow field around a blunt body of revolution in the case of small angles of attack, the relative accuracy in determining the lift coefficient is much less than the relative accuracy in determining the drag coefficient.

The use of the small parameter method imposes two restrictions on the 3-D solution:

(1) a 3-D solution is continuously differentiable with respect to ϵ in the neighborhood of $\epsilon = 0$; and
(2) singularities of the 3-D solution (shock waves, contact discontinuities etc.) must correspond to the singularities of the corresponding axisymmetric solution:

and the following restriction on the angle of attack,

$$\epsilon \cdot \left| \frac{z}{r_w} + \frac{\partial r_w}{\partial z} \right| \ll 1. \tag{10}$$

If the above conditions are satisfied, the small parameter method enables one to find a one-parameter family of solutions, this parameter being the angle of attack.

The small parameter method may be used for simulation of the reverse flows in the ξ-direction, but neither the method of global iterations described in the present paper nor the FVSL equations can be used for modeling reverse flows. As a consequence, only unseparated flows are considered in this study.

NUMERICAL METHOD OF SOLUTION

A new numerical method based on global iterations was developed to solve both the axisymmetric and linearized sets of equations. It is known that the FVSL equations are elliptic in the regions where $u < a$ (a—sonic speed). These regions always exist near the body, since no-slip conditions are imposed on the body surface.

To take into account the elliptic effects of the $\partial y_s/\partial\xi$ and $\partial P/\partial\xi$ terms, the method of global iterations [5] is used. The global iterations approach was originally developed by R. T. Davis [1]. In the method proposed by Davis the FVSL equations are solved iteratively. The global iterations were carried out with respect ot the shock standoff distance y_s and the normal component of the velocity vector v in the n-momentum equation. The shock location was found from the previous global iteration by using the integral mass balance relation in the shock layer. This global iterations method led to good predictions in the case of a thin shock layer.

In the present work the global iterations are carried out in another way [5]. The term $\partial P/\partial\xi$ in the ξ-momentum at each global iteration is represented as

$$\frac{\partial P}{\partial\xi} = \alpha_c \frac{\partial P_c}{\partial\xi} + (1-\alpha_c)\frac{\partial P_g}{\partial\xi}. \tag{11}$$

The FVSL equations are parabolic and the Cauchy problem for the coordinate ξ is correct at each global iteration, if

$$0 \leqslant \alpha_c \leqslant \frac{u^2}{a^2}, \quad u \geqslant 0.$$

To account for the disturbance propagation in the upstream direction, forward differences are used for calculating the terms $(P_g^{(1)})'_\xi$ and $(y_s^{(1)})'_\xi$ in the case of the linearized set of equations and central differences are applied for evaluating the terms $(P_{0g})'_\xi$ and $(y_{0s})'_\xi$ in the case of the axisymmetric equations.

The method of global iterations with respect to the tangential component of the pressure gradient was first developed and employed in Ref. [6] in the treatment of flows with thin subsonic regions. Organized in this way the global iterations are efficient because they enable one to simulate more accurately the upstream propagation of disturbances.

The calculation of the current global iteration in the present method is carried out using the quantities P_g and β_s obtained from the previous global iteration. For the next global iteration the pressure distribution and the shock wave angle are found from

$$\begin{aligned} P_g^{(m+1)} &= \tau_p P_c^{(m)} + (1-\tau_p)P_g^{(m)} \\ \beta_s^{(m+1)} &= \tau_s \beta_s^c + (1-\tau_s)\beta_s^{(m)}, \end{aligned} \tag{12}$$

where β_s^c and $P_c^{(m)}$ represent the shock wave angle and pressure distribution, respectively, and are obtained from the mth global iteration; τ_p and τ_s are the relaxation parameters. From the stability condition of the iteration process for both the pressure and the shock wave angle, the following conditions on τ_p and τ_s are derived: $0 < \tau_p < 2$; $0 < \tau_s < \Delta\xi/y_s$.

In calculating the flow field in the nose region, the shock wave angle was found by using the Rankine–Hugoniot boundary condition (5) for a normal component of the velocity vector v_s. The boundary condition for v_s is not used in calculating the current global iteration and can therefore be used for the determination of the shock location for the next global iteration. We note in passing that it is not clear how to calculate the shock location using the integral mass balance relation in the 3-D case.

To avoid the adverse effects of the discontinuity in the body curvature æ at the sphere–cone tangent point x_c, the following procedure (capable of accounting exactly for this discontinuity) was used:

$$\left[\frac{1}{H_1^2}\cdot\frac{\partial^2 f}{\partial x^2}+\frac{1}{H_1 H_2^2}\cdot\frac{\partial H_1}{\partial\varphi}\cdot\frac{\partial f}{\partial\varphi}+\frac{1}{H_1}\cdot\frac{\partial H_1}{\partial y}\cdot\frac{\partial f}{\partial y}\right]=0,$$

$$[f(x,\varphi,y)]=f(x_c+0,\varphi,y)-f(x_c-0,\varphi,y).$$

The present method of global iterations was used uniformly both for the blunted and conic parts of the body.

To obtain the solution of the linearized set of equations, the initial conditions in the plane $\xi=0$ are needed. The solution begins on the spherically blunted nose by obtaining an axisymmetric solution in the wind-fixed coordinate system, where $\xi'=0$ at the stagnation point. The axisymmetric solution is rotated into a body-fixed coordinate system, where $\xi=0$ at the nosetip of the cone. Following this, the small parameter method is applied to the resulting 3-D solution. The initial conditions for the linearized set of equations are obtained after splitting the 3-D solution into an axisymmetric solution and a linear disturbance, the latter being represented as a Fourier series expansion (7). These conditions are:

$$w^{(1)}|_{\xi=0}=-\left.\frac{\partial u_0}{\partial\xi}\right|_{\xi=0};\quad u^{(1)}|_{\xi=0}=\left.\frac{\partial u_0}{\partial\xi}\right|_{\xi=0};\quad F^{(1)}|_{\xi=0}=0;$$

$$F^{(1)}=\{v^{(1)},y_s^{(1)},P^{(1)},H^{(1)}\}.$$

For the calculation of large-Reynolds-number flows, the adaptive grid approach to the solution in the normal direction is used. The grid step size at each point is chosen in accordance with the values of $\partial u/\partial n$ and $\partial^2 u/\partial n^2$ [7]. This allows one to calculate the flow field over a wide Reynolds number range ($10^2\leqslant \mathrm{Re}_\infty\leqslant 10^7$).

FINITE-DIFFERENCE METHOD

To solve the differential set of equations at each global iteration the following finite-difference method is used.

The non-linear set of equations is solved by using the Newton–Raphson method. At each Newton–Raphson iteration the Gauss–Seidel algorithm is applied. At each point the equations are solved in the following order: (1) ξ-momentum; (2) v-momentum; (3) energy; (4) the coupled continuity and normal momentum equations.

We employ the same finite-difference scheme to solve the ξ-momentum, v-momentum and energy equations. These equations are represented in the standard parabolic form

$$a(f)\cdot\frac{\partial f}{\partial\xi}+b(f)\cdot\frac{\partial f}{\partial n}=\frac{\partial}{\partial n}\left(d(f)\cdot\frac{\partial f}{\partial n}\right)+c(f)\cdot f+e(f),\tag{13}$$

where the coefficients a, b, c, d and e are taken from the previous Newton–Raphson iteration.

The $\partial/\partial\xi$ derivatives are evaluated using a three-step implicit finite-difference Richardson scheme [8]. The first step is defined by

$$a^{n+1}(\bar f)\cdot\frac{f^{n+1}-f^n}{\Delta\xi}+b^{n+1}(\bar f)\left(\frac{\partial f}{\partial n}\right)^{n+1}=\frac{\partial}{\partial n}\left(d(\bar f)\frac{\partial f}{\partial n}\right)^{n+1}+c^{n+1}(\bar f)f^{n+1}+e^{n+1}(\bar f).\tag{14}$$

The second step is defined by

$$a^{n+1/2}(f)\cdot\frac{f^{n+1/2}-f^n}{\Delta\xi/2}+b^{n+1/2}(f)\left(\frac{\partial f}{\partial n}\right)^{n+1/2}=\frac{\partial}{\partial n}\left(d(f)\frac{\partial f}{\partial n}\right)_+^{n+1/2}c^{n+1/2}(\bar f)f^{n+1/2}+e^{n+1/2}(\bar f)\tag{15}$$

$$a^{n+1}(\bar f)\cdot\frac{\bar f^{n+1}-f^{n+1/2}}{\Delta\xi/2}+b^{n+1}(\bar f)\left(\frac{\partial\bar f}{\partial n}\right)^{n+1}=\frac{\partial}{\partial n}\left(d(\bar f)\frac{\partial\bar f}{\partial n}\right)^{n+1}+c^{n+1/2}(\bar f)\bar f^{n+1}+e^{n+1}(\bar f).\tag{16}$$

In the third step, the resulting solution in the $(n+1)$th ξ-section is calculated from

$$f^{n+1} = 2\bar{f}^{n+1} - \bar{f}^{n+1}. \tag{17}$$

The normal derivatives are approximated by the fourth-order finite-difference method [9].

The coupled continuity and normal momentum equations are solved using a finite-difference method which generalizes the Petukhov approximation [9] for sets of hyperbolic equations. The tangential derivatives in the continuity and normal momentum equations are approximated by using the same method as in the case of the parabolic equations (ξ, v-momentum and energy). Therefore, at a section $\xi = \text{const}$, the coupled continuity and normal momentum equations are written in the form of the ordinary differential equations

$$(A \cdot \mathbf{U} + \mathbf{R}_1)'_n = B \cdot \mathbf{U} + \mathbf{R}_2), \tag{18}$$

with boundary conditions of the form

$$\begin{aligned} &(\mathbf{E}_w, \mathbf{U}) = 0, \quad \text{at} \quad n = 0, \ \mathbf{E}_w = \begin{pmatrix} 1 \\ 0 \end{pmatrix} \\ &(\mathbf{E}_s, \mathbf{U}) = 0, \quad \text{at} \quad n = 1, \ \mathbf{E}_s = \begin{pmatrix} 0 \\ 1 \end{pmatrix}. \end{aligned} \tag{19}$$

To solve the boundary problem (18, 19), the coupled continuity and normal momentum equations are integrated from n_i to n_{i+1} $(i = \overline{1, N-1})$ by using Simpson's method:

$$\int_{n_i}^{n_{i+1}} \mathbf{U}\, dn = \frac{\Delta n_i}{3} \cdot (\mathbf{U}_i + 4 \cdot \mathbf{U}_{i+1/2} + \mathbf{U}_{i+1}) + O(\Delta n_i^5), \tag{20}$$

where Δn_i is the half step size of the computational non-uniform grid. The value $U_{i+1/2}$ is eliminated from equation (20) using

$$\mathbf{U}_{i+1/2} = \frac{\mathbf{U}_i + \mathbf{U}_{i+1}}{2} - \frac{\Delta n_i}{4} \cdot ((\mathbf{U}'_n)_{i+1} - (\mathbf{U}'_n)_i) + O(\Delta n_i^4), \tag{21}$$

where the derivatives $[\mathbf{U}'_n)_{i+1}$ and $(\mathbf{U}'_n)_i$ are calculated from equations (18).

The set of finite-difference equations complemented with the boundary conditions may be written as

$$a_{i+1/2}\mathbf{U}_i + b_{i+1/2}\mathbf{U}_i = r_{i+1/2} \quad (i = \overline{1, M}) \tag{22}$$

and

$$(E_w, \mathbf{U}_1) = 0; \quad (E_s, \mathbf{U}_M) = 0, \tag{23}$$

where the matrixes $a_{i+1/2}$ and $b_{i+1/2}$ are

$$a_{i+1/2} = A_i + \frac{\Delta n_i}{3}(B_i + 2 \cdot B_{i+1/2} A_{i+1/2}^{-1} A_i) + \frac{\Delta n_i^2}{3} \cdot B_{i+1/2} A_{i+1/2}^{-1} B_i$$

and

$$b_{i+1/2} = A_{i+1} + \frac{\Delta n_i}{3}(B_{i+1} - 2 \cdot B_{i+1/2} A_{i+1/2}^{-1} A_{i+1}) + \frac{\Delta n_i^2}{3} \cdot B_{i+1/2} A_{i+1/2}^{-1} B_{i+1}.$$

Equations (22) and (23) are solved as follows. At each grid point equations (22) and (23) are represented as

$$\mu_m \mathbf{U}_m = G_m. \tag{24}$$

Multiplying both sides of equation (24) by μ_m at point $i = m$, equation (24) may be written as

$$\mu_{m+1}\mathbf{U}_{m+1} = G_{m+1}, \quad \mu_{m+1} = \rho_m \mu_m b_{m+1/2}^{-1} a_{m+1/2}, \tag{25}$$

$$G_{m+1} = \rho_m(\mu_m b_{m+1/2}^{-1} r_{m+1/2} - G_m) \tag{26}$$

and

$$\rho_m^{-1} = \|\mu_m b_{m+1/2}^{-1} a_{m+1/2}\|. \tag{27}$$

The set of equations (25) at point $i = M$ is completed by adding the boundary conditions. The extended set of equations is solved for $\mathbf{U}_M$. The values $\mathbf{U}_i$ $(i = \overline{2, M-1})$ are found from

$$\mathbf{U}_{i-1} = P_{i-1}\mathbf{U}_i + \mathbf{Q}_{i-1} \quad (i = \overline{2, M}), \tag{28}$$

where

$$P_{i-1} = -(T_1 b_{i-1/2} + T_2 \mu_{i-1})^{-1} T_1 a_{i-1/2},$$
$$a_{i-1} = (T_1 b_{i-1/2} + T_2 \mu_{i-1})^{-1}(T_1 r_{i-1/2} + T_2 G_{i-1}),$$
$$T_1 = \begin{pmatrix} 1 & 0 \\ 0 & 0 \end{pmatrix}, \quad T_2 = \begin{pmatrix} 0 \\ 1 \end{pmatrix}.$$

The described algorithm for the solution of equations of the type (22, 23) with a bidiagonal matrix was originally developed by V. V. Rusanov [10]. Algorithm (28) is stable in the case of coupled and normal momentum equations. The present approach is advantageous in that it is of the fourth order in the normal coordinate and provides a simple way to specify the appropriate boundary conditions (in particular, no artificial conditions, such as $P_n'|_w = 0$, are needed).

Thus, the finite-difference method we propose is of the second order in the tangential coordinate and of the fourth order in the normal coordinate.

The same finite-difference approximation scheme for normal derivatives, combined with an ordinary first-order implicit scheme for the tangential coordinate, are used for the solution of the linearized set of equations (the use of a first-order implicit scheme is justified by the fact that the approximation error is multiplied by the small parameter ϵ).

RESULTS AND DISCUSSION

The present method was used to compute the perfect gas flow past cones and past a biconic body at various angles of attack. The cone half-angles are varied from 5° to 45° and the angles of attack from 2° to 10°. The values of γ and the Prandtl number are taken as 1.4 and 0.72, respectively.

Figure 1 shows the comparison of the shock standoff distance, for a 25° half-angle cone at a 10° angle of attack, with the experimental results [11]. For a blunt body at angle of attack, the leeward shock standoff distance is expected to be larger than that on the windward side. This is seen clearly in Fig. 1 for a 25° half-angle cone. The experimental results exhibit the same behavior. In this case, the free-stream conditions are: $M_\infty = 5.9$, $T_w = 0.7$ K, $T_\infty = 53.7$ K, $Re_\infty = 3.95 \times 10^4$, $\epsilon = 10°$, $\theta_c = 25°$.

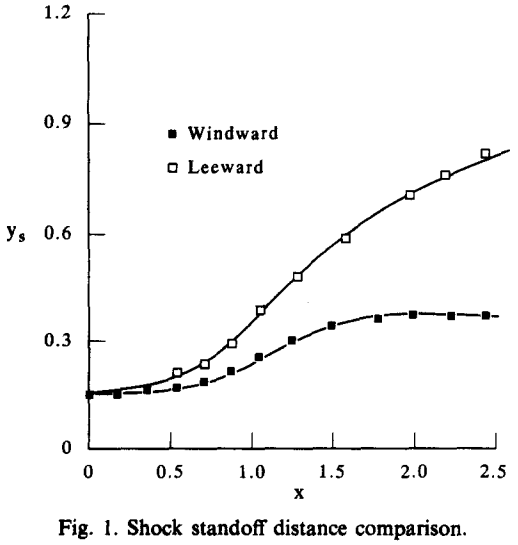

Fig. 1. Shock standoff distance comparison.

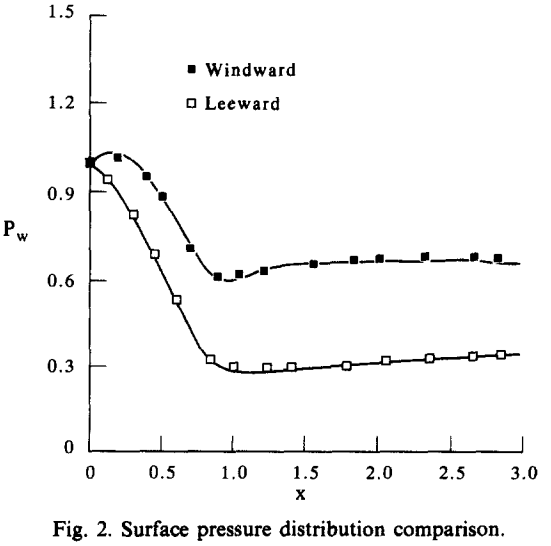

Fig. 2. Surface pressure distribution comparison.

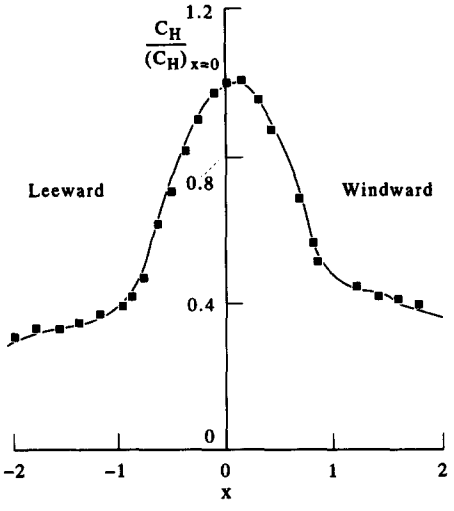

Fig. 3. Heat transfer comparison.

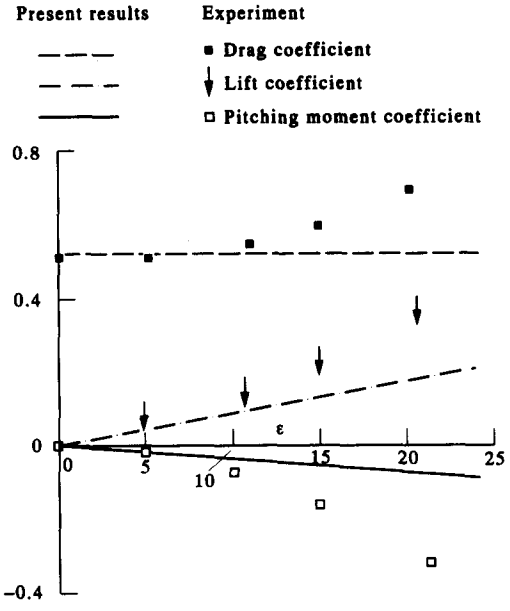

Fig. 4. Comparison of drag, lift and pitching moment coefficients with the experimental results.

Figure 2 compares the surface pressure distribution computed by the present method with the experimental data [12]. The free-stream flow conditions are: $M_\infty = 5.8$, $T_w = 300$ K, $T_0 = 428$ K, $Re_\infty = 3.95 \times 10^4$, $\epsilon = 8°$, $\theta_c = 40°$.

In Fig. 3 the present heating-rate results for a 45° half-angle cone at a 5° angle of attack are compared with the experimental data [13]. The free-stream conditions are: $M_\infty = 10.33$, $T_w = 0.701$ K, $T_\infty = 46.82$ K, $Re_\infty = 1.13 \times 10^5$, $\theta_c = 45°$, $\epsilon = 5°$.

For all the examples above, the deviation from the experimental results is about 5%.

In Fig. 4, the drag, lift and pitching moment coefficients at the point $z = 6.98$ are compared with the experimental results of Ref. [14] for a 5° half-angle cone at angles of attack varying from 0° to 20°. The free-stream conditions are: $Re_\infty = 4.1 \times 10^3$, $M_\infty = 13$, $H_w = 0.27$, $p = 0.75$ (the power in the viscosity law). From the theoretical results (10), it follows that the small parameter method is valid in this case only for $\epsilon < 5°$. Nevertheless, as is seen from Fig. 4, the present results compare well with the experiental data up to angles of attack of about 10°. Hence, as far as the integrated characteristics of the flow are concerned, the small parameter method is valid for a broader range of angles of attack than is predicted from the theoretical considerations.

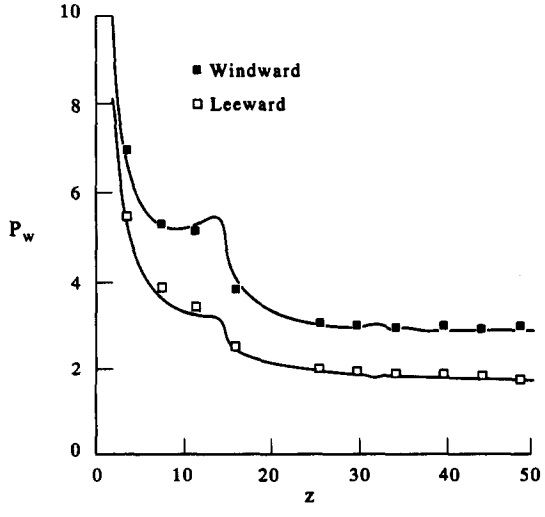

Fig. 5. Surface pressure comparison.

Figure 5 compares the windward and leeward surface pressure distributions on a blunt biconic computed by the present method with the experimental results [15]. For calculation of the flow field around a long blunt biconic at an angle of attack the block-marching method is used. The entire computational domain is divided into a number of intersecting blocks. For the calculation of each of these blocks, the method of global iterations is used. Block intersection is used for the propagation of the disturbances in the upstream direction in the subsonic flow regions. To calculate the viscous shock layer near the cone–cone junction, where the body-oriented coordinate system has a singularity, a smoothing of the body surface angle α is applied. The smoothing covers only about 4–5 points of the computational grid in the ξ-direction. To calculate the cone–cone junction region more accurately, the grid is adapted in both the n- and ξ-directions. The free-stream conditions in this case are: $\mathrm{Re}_\infty = 3.5 \times 10^4$, $\mathrm{M}_\infty = 10.1$, $T_\infty = 159.8$ K, $H_w = 0.705$, $\theta_{c1} = 9.33$, $\theta_{c2} = 5°$, $\epsilon = 2°$. The calculated results compare well with the experimental data [15].

CONCLUDING REMARKS

To obtain the solutions for both the axisymmetric and linearized sets of equations, only about 10 global iterations on the nose part and about 3 global iterations on the conic part of the body were needed.

Comparison of this approach with the implicit time-marching method has shown that, with no loss of accuracy, the time necessary for the calculation in the 3-D case is about 100 times less. In addition, the small parameter method makes it possible to find a one-parameter family of solutions. The angle of attack is the parameter.

The numerical results of the present analysis for quantities such as the shock standoff distance, surface pressure distribution and heating rates compare well with the theoretical and experimental results available in the literature. The calculation time remains virtually unchanged for a wide range of Mach numbers ($\mathrm{M}_\infty > 3$) and Reynolds numbers ($10^2 \leqslant \mathrm{Re}_\infty \leqslant 10^7$).

The numerical results were obtained on a PC/AT-386. The computing time was about 30 min for the 3-D cases and about 15 min for axisymmetric cases. Although we only considered spherically blunted cones and biconics in this study, the analysis can be applied to other axisymmetric spherically blunted bodies at angles of attack without any modifications.

REFERENCES

1. R. T. Davis, Numerical solution of the hypersonic viscous shock-layer equations. *AIAA Jl* **8**(5), 843 (1970).
2. L. I. Sedov, *Mechanics of Continua*, Vol. 1. Nauka, Moscow (1983).
3. A. H. Stone, On supersonic flow past a slightly yawing cone. *J. Math. Phys.* **27**(1), 67 (1948).
4. V. E. Karyakin, Calculation of supersonic viscous gas flow over body of revolution at small angle of attack. *J. Comput. Math. Math. Phys.* **21**(1), 150 (1981). In Russian.
5. S. A. Vasilyevskii, G. A. Tirskii and S. V. Utyuzhnikov, Numerical method for solution of viscous shock-layer equations. *J. Comput. Math. Math. Phys.* **27**(5), 741 (1987). In Russian.
6. A. Lin and S. G. Rubin, Three-dimensional supersonic viscous flow over cone at incidence. AIAA Paper 192 (1981).
7. H. A. Dwyer, Grid adaption for problems in fluid dynamics. *AIAA Jl* **22**(12), 1705 (1984).
8. L. F. Richardson, The approximate arithmetical solution by finite differences of physical problems involving differential equations, with an application to the stress in a masonary dam. *Phil. Trans. R. Soc. Lond.* **A210** (1910).
9. I. V. Petukhov, Numerical calculation of two-dimensional flows with boundary layers. In *Trans. on Numerical Methods of Solution of Differential and Integral Equations*, pp. 304–325. Nauka, Moscow (1964). In Russian.
10. A. N. Lubimov, V. V. Rusanov, *The Gas Flow Near Blunted Bodies*, Vol. 1. Nauka, Moscow (1970). In Russian.
11. F. Marconi, L. Yaeger and H. H. Hamilton, Computation of high speed inviscid flows about real configurations. In *Proc. of Aerodynamic Analysis Requiring Advanced Computers*—Part II, SP-347, pp. 1411–1455. NASA, U.S.A. (1975).
12. W. T. O'Bryant and R. M. Machell, An experimental investigation of flow over blunt nosed cones at a Mach number of 5.8. *J. Aerospace Sci.* **23**(11), 1054 (1956).
13. A. Kumar and R. A. Graves, Numerical solution of the viscous hypersonic flow past blunted cones at angle of attack. AIAA Paper 172 (1977).
14. V. M. Kovenya, G. A. Tarnavskii and S. G. Cherny, *The Application of Splitting Methods to Aerodynamics Problems*. Nauka, Novosibirsk (1990).
15. A. W. Mayne, Calculation of the laminar viscous shock layer on a blunt biconic body at incidence to supersonic and hypersonic flow. AIAA Paper 77–88 (1977).

APPENDIX

The linearized set of equations is:

$$\frac{\partial}{\partial\xi}\left[H_{02}\rho_0 u^{(1)}+H_{02}\rho^{(1)}u_0+H_2^{(1)}\rho_0 u_0\right]+H_{01}\rho_0 w^{(1)}-\frac{n}{y_{0s}}\cdot\frac{\partial y_{0s}}{\partial\xi}\frac{\partial}{\partial n}\left[H_{02}\rho_0 u^{(1)}+H_{02}\rho^{(1)}u_0+H_2^{(1)}\rho_0 u_0\right]$$
$$-\frac{n}{y_{0s}}\left[\frac{\partial y_s^{(1)}}{\partial\xi}-\frac{\partial y_{0s}}{\partial\xi}\frac{y_s^{(1)}}{y_{0s}}\right]\frac{\partial}{\partial n}\left(H_{02}\rho_0 u_0\right)+\frac{1}{y_{0s}}\cdot\frac{\partial}{\partial n}\left[H_{01}H_{02}\rho_0 v^{(1)}+H_{01}H_{02}\rho^{(1)}v_0\right.$$
$$\left.+H_{01}H_2^{(1)}\rho_0 v_0+H_1^{(1)}H_{02}\rho_0 v_0\right]-\frac{y_s^{(1)}}{y_{0s}^2}\frac{\partial}{\partial n}\left[H_{01}H_{02}\rho_0 v_0\right]=0,$$

$$\rho_0 D_F^{*}\mu+\rho^{(1)}D_0^{*}u+\frac{1}{y_{0s}H_{01}}\cdot\frac{\partial H_{01}}{\partial n}\left(u_0v^{(1)}\rho_0+u^{(1)}v_0\rho_0+u_0v_0\rho^{(1)}\right)+\frac{u_0v_0\rho_0}{y_{0s}H_{01}}\cdot\frac{\partial H_1^{(1)}}{\partial n}-\frac{u_0v_0\rho_0}{y_{0s}H_{01}}\cdot\frac{\partial H_{01}}{\partial n}\left(\frac{H_1^{(1)}}{H_{01}}+\frac{y_s^{(1)}}{y_{0s}}\right)$$
$$=-\frac{1}{H_{01}}\left[\frac{\partial P^{(1)}}{\partial\xi}-\frac{n}{y_{0s}}\cdot\frac{\partial y_{0s}}{\partial\xi}\cdot\frac{\partial P^{(1)}}{\partial n}-\frac{n}{y_{0s}}\cdot\frac{\partial y_s^{(1)}}{\partial\xi}\cdot\frac{\partial P_0}{\partial n}+\frac{ny_s^{(1)}}{y_{0s}^2}\cdot\frac{\partial y_{0s}}{\partial\xi}\cdot\frac{\partial P_0}{\partial n}\right]+\frac{H_1^{(1)}}{H_{01}^2}\left[\frac{\partial P_0}{\partial\xi}-\frac{n}{y_{0s}}\cdot\frac{\partial y_{0s}}{\partial\xi}\cdot\frac{\partial P_0}{\partial n}\right]$$
$$+\frac{1}{H_{01}^2H_{02}\mathrm{Re}_\infty y_{0s}^2}\left\{\frac{\partial}{\partial n}\left[H_{01}^3H_{02}\mu_0\cdot\frac{\partial}{\partial n}\left(\frac{u^{(1)}}{H_{01}}-\frac{u_0H_1^{(1)}}{H_{01}^2}\right)+\left(3H_{01}^2H_1^{(1)}H_{02}\mu_0+H_{01}^3H_2^{(1)}\mu_0\right.\right.\right.$$
$$\left.\left.\left.+H_{01}^3H_{02}\mu^{(1)}\right)\cdot\frac{\partial}{\partial n}\left(\frac{u_0}{H_{01}}\right)\right]-\left(\frac{2H_1^{(1)}}{H_{01}}+\frac{H_2^{(1)}}{H_{02}}+\frac{2y_s^{(1)}}{y_{0s}}\right)\cdot\frac{\partial}{\partial n}\left[H_{01}^3H_{02}\mu_0\frac{\partial}{\partial n}\left(\frac{u_0}{H_{01}}\right)\right]\right\},$$

$$\rho_0 D_F^{*}v+\rho^{(1)}D_0^{*}v-\frac{2u_0u^{(1)}\rho_0}{y_{0s}H_{01}}\cdot\frac{\partial H_{01}}{\partial n}-\frac{\rho_0u_0^2}{y_{0s}H_{01}}\cdot\frac{\partial H_1^{(1)}}{\partial n}-\frac{\rho^{(1)}u_0^2}{y_{0s}H_{01}}\cdot\frac{\partial H_{01}}{\partial n}+\frac{\rho_0u_0^2}{y_{0s}H_{01}}\cdot\frac{\partial H_{01}}{\partial n}\left(\frac{H_1^{(1)}}{H_{01}}+\frac{y_s^{(1)}}{y_{0s}}\right)$$
$$=-\frac{1}{y_{0s}}\cdot\frac{\partial P^{(1)}}{\partial n}+\frac{y_s^{(1)}}{y_{0s}^2}\cdot\frac{\partial P_0}{\partial n},$$

$$\rho_0 D_F^{*}w+\frac{u_0\rho_0w^{(1)}}{H_{01}H_{02}}\left(\frac{\partial H_{02}}{\partial\xi}-\frac{n}{y_{0s}}\cdot\frac{\partial y_{0s}}{\partial\xi}\cdot\frac{\partial H_{02}}{\partial n}\right)+\frac{u_0^2\rho_0}{H_{01}H_{02}}\left(H_1^{(1)}-\frac{ny_s^{(1)}}{y_{0s}}\cdot\frac{\partial H_{01}}{\partial n}\right)+\frac{v_0\rho_0w^{(1)}}{y_{0s}H_{02}}\cdot\frac{\partial H_{02}}{\partial n}$$
$$=-\frac{1}{H_{02}}\left[-P^{(1)}+\frac{ny_s^{(1)}}{y_{0s}}\cdot\frac{\partial P_0}{\partial n}\right]+\frac{1}{H_{01}H_{02}^2\mathrm{Re}_\infty y_{0s}^2}\cdot\frac{\partial}{\partial n}\left[H_{01}H_{02}^3\mu_0\frac{\partial}{\partial n}\left(\frac{w^{(1)}}{H_{02}}\right)\right],$$

$$\rho_0 D_F^{*}H+\rho^{(1)}D_0^{*}H=\frac{1}{H_{01}H_{02}^2\mathrm{Re}_\infty y_{0s}^2}\cdot\left\{\frac{\partial}{\partial n}\left[\frac{\mu_0H_{01}H_{02}}{\sigma}\cdot\left\{\left(\frac{H_1^{(1)}}{H_{01}}+\frac{H_2^{(1)}}{H_{02}}+\frac{\mu^{(1)}}{\mu_0}\right)L_0+\frac{\partial H^{(1)}}{\partial n}\right.\right.\right.$$
$$\left.\left.+\frac{V_\infty^2}{H_\infty}\left((\sigma-1)\cdot\left[u_0\cdot\frac{\partial u^{(1)}}{\partial n}+u^{(1)}\cdot\frac{\partial u_0}{\partial n}\right]-\frac{\sigma u_0^2}{H_{01}}\cdot\frac{\partial H_1^{(1)}}{\partial n}-\frac{2\sigma u_0u^{(1)}}{H_{01}}\cdot\frac{\partial H_{01}}{\partial n}+\frac{\sigma u_0^2H_1^{(1)}}{H_{01}^2}\cdot\frac{\partial H_{01}}{\partial n}\right)\right\}\right]$$
$$\left.-\left(\frac{H_1^{(1)}}{H_{01}}+\frac{H_2^{(1)}}{H_{02}}+\frac{2y_s^{(1)}}{y_{0s}}\right)\cdot\frac{\partial}{\partial n}\left[\frac{\mu_0H_{01}H_{02}}{\sigma}L_0\right]\right\}$$

and

$$h^{(1)}=\frac{V_\infty^2}{H_\infty}\cdot\left(\frac{\gamma}{\gamma-1}\cdot\frac{P^{(1)}}{\rho_0}-\frac{P_0\gamma}{\gamma-1}\cdot\frac{\rho^{(1)}}{\rho_0^2}\right).$$

Where D_F^{*}, $H_1^{(1)}$ and $H_2^{(1)}$ are given as follows:

$$D_F^{*}F=\frac{u_0}{H_{01}}\cdot\frac{\partial F^{(1)}}{\partial\xi}+\left(\frac{v_0}{y_{0s}}-\frac{u_0n}{H_{01}y_{0s}}\frac{\partial y_{0s}}{\partial\xi}\right)\frac{\partial F^{(1)}}{\partial n}+\frac{\partial F_0}{\partial\xi}\left(\frac{u^{(1)}}{H_{01}}-u_0\cdot\frac{H_1^{(1)}}{H_{01}^2}\right)$$
$$+\frac{\partial F_0}{\partial n}\cdot\left\{\frac{v^{(1)}}{y_{0s}}-\frac{v_0y_s^{(1)}}{y_{0s}^2}-\frac{n}{H_{01}y_{0s}}\left(u_0\frac{\partial y_s^{(1)}}{\partial\xi}-u_0\frac{\partial y_{0s}}{\partial\xi}\frac{y_s^{(1)}}{y_{0s}}\right.\right.$$
$$\left.\left.-u_0\frac{\partial y_{0s}}{\partial\xi}\cdot\frac{H_1^{(1)}}{H_{01}}+u^{(1)}\cdot\frac{\partial y_{0s}}{\partial\xi}\right)\right\};\quad F=\{u,v,H\},$$

$$D_F^{*}w=\frac{u_0}{H_{01}}\frac{\partial w^{(1)}}{\partial\xi}+\left(\frac{v_0}{y_{0s}}-\frac{u_0n}{H_{01}y_{0s}}\frac{\partial y_{0s}}{\partial\xi}\right)\frac{\partial w^{(1)}}{\partial n}$$

and

$$H_1^{(1)}=n\cdot y_s^{(1)}\cdot\varkappa;\quad H_2^{(1)}=n\cdot y_s^{(1)}\cdot\cos\alpha.$$

The Rankine–Hugoniot conditions are:

$$v_s^{(1)} = \frac{u_{0s}}{\cos^2 \beta_{0s}} \beta_s^{(1)} + u_s^{(1)} \tan \beta_{0s} + K_{0s} \cdot V_\infty^{(1)}(3) + K_s^{(1)} \cdot V_{0\infty}(3),$$

$$u_s^{(1)} = V_\infty^{(1)}(1)\cos^2 \beta_{0s} - \beta_s^{(1)}(V_{0\infty}(1) \cdot \sin 2\beta_{0s} + K_{0s} \cdot V_{0\infty}(3)\cos 2\beta_{0s}) - \frac{K_{0s}}{2} \cdot V_\infty^{(1)}(3) \cdot \sin 2\beta_{0s} - \frac{V_{0\infty}(3)}{2} \cdot \sin 2\beta_{0s} \cdot K_s^{(1)}$$
$$+ \frac{\mu_{0s}}{\mathrm{Re}_\infty V_{0\infty}(3) y_{0s}} \left(\frac{\partial u^{(1)}}{\partial n} - \frac{u_0}{H_{01}} \cdot \frac{\partial H_1^{(1)}}{\partial n} - \frac{u^{(1)}}{H_{01}} \cdot \frac{\partial H_{01}}{\partial n} + \frac{u_0 H_1^{(1)}}{H_{01}^2} \cdot \frac{\partial H_{01}}{\partial n} \right)_s$$
$$+ \frac{\mu_{0s}}{\mathrm{Re}_\infty V_{0\infty}(3) y_{0s}} \left(\frac{\mu^{(1)}}{\mu_0} - \frac{y_s^{(1)}}{y_{0s}} - \frac{V_\infty^{(1)}(3)}{V_{0\infty}(3)} \right)_s \cdot \left[\frac{\partial u_0}{\partial n} - \frac{\partial H_{01}}{\partial n} \right]_s,$$

$$w_s^{(1)} = V_\infty^{(1)}(2) - (u_{0s} \tan \beta_{0s} + K_{0s} V_{0\infty}(3))\gamma_s^{(1)} + \frac{\mu_{0s}}{\mathrm{Re}_\infty V_{0\infty}(3) y_{0s}} \left(\frac{\partial w^{(1)}}{\partial n} - \frac{w^{(1)}}{H_{02}} \cdot \frac{\partial H_{02}}{\partial n} \right)_s,$$

and

$$H_s^{(1)} = \frac{\mu_{0s}}{\sigma \mathrm{Re}_\infty V_{0\infty}(3) y_{0s}^2} \cdot \left\{ \frac{\partial H^{(1)}}{\partial n} + \frac{V_\infty^2}{H_\infty} \left((\sigma - 1) \left[u_0 \frac{\partial u^{(1)}}{\partial n} + u^{(1)} \frac{\partial u_0}{\partial n} \right] \right.\right.$$
$$\left.\left. - \frac{\sigma u_0^2}{H_{01}} \cdot \frac{\partial H_1^{(1)}}{\partial n} - \frac{2\sigma u_0 u^{(1)}}{H_{01}} \cdot \frac{\partial H_{01}}{\partial n} + \frac{\sigma u_0^2 H_1^{(1)}}{H_{01}^2} \cdot \frac{\partial H_{01}}{\partial n} \right) + \left(\frac{\mu^{(1)}}{\mu_0} - \frac{V_\infty^{(1)}(3)}{V_{0\infty}(3)} - \frac{y_s^{(1)}}{y_{0s}} \right)_s \cdot L_{0s} \right\}$$

Where

$$\beta_s^{(1)} = \frac{\cos^2 \beta_{0s}}{H_{01_s}} \left(\frac{\partial y_s^{(1)}}{\partial \xi} - \frac{H_{1s}^{(1)}}{H_{01}} \cdot \frac{\partial y_{0s}}{\partial \xi} \right)_s$$

$$\gamma_s^{(1)} = -\frac{1}{H_{02_s}} \cdot y_s^{(1)}; \quad K_s^{(1)} = -\frac{\rho_s^{(1)}}{\rho_{0s}^2},$$

$$V_\infty^{(1)}(1) = \sin \alpha + \tan \beta_{0s} \cdot \cos \alpha - \frac{\sin \alpha}{\cos^2 \beta_{0s}} \cdot \beta_s^{(1)},$$

$$V_s^{(1)}(2) = -\sin \nu - \gamma_s^{(1)} \cdot \sin \alpha$$

and

$$V_\infty^{(1)}(3) = \cos \alpha - \tan \beta_{0s} \cdot \sin \alpha - \frac{\cos \alpha}{\cos^2 \beta_{0s}} \beta_s^{(1)}.$$

The body surface conditions are:

$$u_w^{(1)} = w_w^{(1)} = v_w^{(1)} = 0$$

and

$$H_w^{(1)} = 0.$$